A homogenization approach for the limit analysis of out-of-plane loaded masonry walls

Gabriele Milani [(1)], Paulo Lourenço [(2)], Antonio Tralli [(3)]

(1) Corresponding Author, PhD, University of Ferrara, Via Saragat 1, 44100 Ferrara Italy. Department of Engineering – University of Ferrara – Via Saragat 1 – 44100 – Ferrara - Italy. e-mail: gmilani@ing.unife.it . Phone: +39 0532 974911. Fax: +39 0532 974870.

(2) Associate Professor, Department of Civil Engineering, School of Engineering, University of Minho, Azurém, 4800-058 Guimarães.

(3) Full Professor, University of Ferrara, Via Saragat 1, 44100 Ferrara Italy

CE Database Headings: Masonry, Finite Elements, Structural Analysis, Constitutive models, Validation

Abstract

This paper addresses the usage of a simplified homogenization technique for the analysis of masonry subjected to out-of-plane loading. The anisotropic failure surface, based on the definition of a polynomial representation of the stress tensor components in a finite number of sub-domains, is combined with finite element triangular elements employed for the upper and lower bound limit analyses. Several comparisons between the proposed model and experimental data available in the literature are presented, for wallettes subjected to bending at different orientations and for different panels loaded out-of-plane. The limit analysis results allow to identify the distribution of internal forces at critical sections and to obtain the collapse modes, as well as the failure loads. Excellent results are found in all cases, indicating that the proposed simple tool is adequate for the safety assessment of out-of-plane loaded masonry panels. The combined usage of upper and lower bound approaches, and their respective simplifications, allow to define a narrow interval for the real collapse load.

1. Introduction

The prediction of the ultimate load bearing capacity of masonry walls out-of-plane loaded is of great relevance for the design of masonry structures. Out-of-plane failures are mostly related to seismic and wind loads and the lack of out-of-plane strength is a primary cause of failure in different forms of masonry, particularly in the case of historical buildings (Spence and Coburn 1992). Masonry structures are often subjected simultaneously to in-plane compressive vertical loads (either self weight and permanent loads) and out-of-plane actions. Such loads increase both the ultimate out-of-plane strength and the ductility of masonry, and bring additional complexity to the structural analysis.

Laboratory tests (e.g. Gazzola et al. 1985, Southcombe et al. 1995) conducted on brick masonry walls subjected to lateral loads, have shown that failure takes place along a well-defined pattern of lines. This has inspired approximate analytical solutions based both on the yield line theory and on the fracture line theory (Sinha 1978). The yield line approach has been adopted by many codes, namely BS 5628 (British Standard Institution, 2005) and Eurocode 6 (CEN, 2004), despite the approximations and knowledge that masonry does not behave as a rigid-plastic material. Therefore, the prediction of masonry ultimate strength under out-of-plane loads is still an open issue and a general model is far from being developed. The major difficulties in masonry modeling are due to masonry heterogeneity, as a regular assemblage of bricks and mortar, and due to the quasi-brittle behavior of joints under tension.

Limit analysis combined with homogenization techniques is a powerful structural analysis tool to predict masonry behavior at collapse. This approach requires only a reduced number of material parameters and allows to avoid independent modeling of units and mortar. In addition, it provides limit multipliers of loads, failure mechanisms and, on critical sections, the stress distribution at collapse. A drawback of homogenization techniques is that, formally, the evaluation of average quantities requires the solution (usually by means of FE techniques) of a

boundary value problem on the elementary cell, so that different loading conditions require different expensive computational simulations.

In this paper, a simplified and efficient model for homogenized limit analysis of out-of-plane loaded masonry structures is presented. In the model, the elementary cell is subdivided along the thickness in several layers. For each layer, fully equilibrated stress fields are assumed, adopting polynomial expressions for the stress tensor components in a finite number of sub-domains, imposing the continuity of the stress vector on the interfaces and defining anti-periodicity conditions on the boundary surface. Furthermore, admissibility constraints are imposed for the constituent materials enforcing the satisfaction of the yield conditions for joints and bricks on a regular grid of points. Even if such stress distribution is not exactly statically admissible in the elementary cell, it has been shown (Milani et al. 2005) that a technically suitable approximation of the homogenized yield surface is obtained using the proposed procedure. Finally, the out-of-plane failure surfaces of masonry so recovered are implemented in FE limit analysis codes (both upper and lower bound) for structural analyses at collapse of entire panels..

2. Modeling approach

Let us consider a masonry wall Ω constituted by a periodic arrangement of bricks and mortar disposed in running bond texture (Figure 1). As it as been shown by Suquet (Suquet 1983) and further detailed for in-plane loaded brickwork (Milani et al. 2005), homogenization techniques combined with limit analysis can be profitably applied for the evaluation of the homogenized out-of-plane strength domain S^{hom} of masonry. Under the assumptions of perfect plasticity and associated flow rule for the constituent materials, and in the framework of the lower bound limit analysis theorem, S^{hom} can be derived by means of the following (non-linear) optimization problem (see also Figure 1):

$$S^{\hom} = \left\{ (\mathbf{M},\mathbf{N}) \middle| \left\{ \begin{array}{rl} \mathbf{N} = \dfrac{1}{|Y|}\displaystyle\int_{Y\times h} \boldsymbol{\sigma} dV & (a) \\ \mathbf{M} = \dfrac{1}{|Y|}\displaystyle\int_{Y\times h} y_3 \boldsymbol{\sigma} dV & (b) \\ div\boldsymbol{\sigma} = \mathbf{0} & (c) \\ [\![\boldsymbol{\sigma}]\!]\mathbf{n}^{\text{int}} = \mathbf{0} & (d) \\ \boldsymbol{\sigma}\mathbf{n} \quad \text{anti-periodic} \quad \text{on} \quad \partial Y_l & (e) \\ \boldsymbol{\sigma}(\mathbf{y}) \in S^m \quad \forall \mathbf{y} \in Y^m \;;\; \boldsymbol{\sigma}(\mathbf{y}) \in S^b \quad \forall \mathbf{y} \in Y^b & (f) \end{array} \right\} \right\} \qquad (1)$$

where:

- $\mathbf{N}$ and $\mathbf{M}$ are the macroscopic in-plane (membrane forces) and out-of-plane (bending moments) tensors;

- $\boldsymbol{\sigma}$ denotes the microscopic stress tensor;

- $\mathbf{n}$ is the outward versor of ∂Y_l surface;

- ∂Y_l is defined in Figure 1**;**

- $[\![\boldsymbol{\sigma}]\!]$ is the jump of micro-stresses across any discontinuity surface of normal $\mathbf{n}^{\text{int}}$;

- S^{m} and S^{b} denote respectively the strength domains of mortar and bricks;

- Y is the cross section of the 3D elementary cell with $y_3 = 0$ (see Figure 1), $|Y|$ is its area, V is the elementary cell, h represents the wall thickness and $y = (y_1 \quad y_2 \quad y_3)$;

- condition (1-c) imposes the micro-equilibrium with zero body forces, which are usually neglected in the framework of the homogenisation theory;

- anti-periodicity condition (1-e) requires that that stress vectors $\boldsymbol{\sigma}\mathbf{n}$ are opposite on opposite sides of ∂Y_l, Figure 2-c, i.e. $\sigma^{(m)}\mathbf{n}_1 = -\sigma^{(n)}\mathbf{n}_2$.

It is stressed that experimental evidences show a typical non-associated behaviour for masonry in the inelastic range. On the other hand, the classical limit analysis theorems lead to simple linear programming problems when associated flow rules for the constituent materials are assumed. Nowadays, such problems can be tackled relatively easily by practitioners making use of both well known simplex-type and interior-point algorithms, which present robust numerical stability and need a very limited computational time for the simulations. Since more

sophisticated tools are required when a non-associated flow rule is assumed for the constituent materials and plastic flow is mostly relevant in the cases that masonry is severely constrained to deform in plane, the classical associated formulation for the plastic flow is assumed in this paper for the sake of simplicity.

2.1. The micro-mechanical model proposed

A simple admissible and equilibrated micro-mechanical model for the evaluation of S^{hom} is here presented. The unit cell is subdivided into a fixed number of layers along its thickness, as shown in Figure 2-a. According to classical limit analysis plate models (see for instance Hodge 1959), for each layer out-of-plane components σ_{i3} $(i = 1, 2, 3)$ of the micro-stress tensor $\boldsymbol{\sigma}$ are set to zero, so that only in-plane components σ_{ij} $(i, j = 1, 2)$ are considered active. Furthermore, σ_{ij} $(i, j = 1, 2)$ are kept constant along the Δ_{i_L} thickness of each layer, i.e. in each layer $\sigma_{ij} = \sigma_{ij}(y_1, y_2)$. For each layer one-fourth of the REV is sub-divided into nine geometrical elementary entities (*sub-domains*), so that the entire cell is sub-divided into 36 sub-domains (see Milani et al. 2005 and Figure 2-b).

For each sub-domain (k) and layer (i_L), simple polynomial distributions of degree *(m)* in the variables (y_1, y_2) are a priori assumed for the stress components. Since stresses are polynomial expressions, the generic *ij*th component can be written as follows:

$$\sigma_{ij}^{(k,i_L)} = \mathbf{X}(\mathbf{y})\mathbf{S}_{ij}^{(k,i_L)T} \quad \mathbf{y} \in Y^{(k,i_L)} \tag{2}$$

where:

- $\mathbf{X}(\mathbf{y}) = \left[1 \quad y_1 \quad y_2 \quad y_1^2 \quad y_1 y_2 \quad y_2^2 \quad \ldots\right]$;
- $\mathbf{S}_{ij}^{(k,i_L)} = \left[S_{ij}^{(k,i_L)(1)} \quad S_{ij}^{(k,i_L)(2)} \quad S_{ij}^{(k,i_L)(3)} \quad S_{ij}^{(k,i_L)(4)} \quad S_{ij}^{(k,i_L)(5)} \quad S_{ij}^{(k,i_L)(6)} \quad \ldots\right]$ is a vector representing the unknown stress parameters of sub-domain (k) of layer (i_L);
- $Y^{(k,i_L)}$ represents the k^{th} sub-domain of layer (i_L).

The imposition of equilibrium inside each sub-domain (with zero body forces, as usual in homogenization procedures), the continuity of the stress vector on interfaces and the anti-periodicity of $\boldsymbol{\sigma}\mathbf{n}$ permit a strong reduction of the number of independent stress parameters.

The imposition of micro-stress equilibrium ($\sigma_{ij,j} = 0 \quad i = 1,2$) in each sub-domain yields:

$$\sum_{j=1}^{2} \mathbf{X}(\mathbf{y})_{,j} \mathbf{S}_{ij}^{(k,i_L)T} = \mathbf{0} \tag{3}$$

If p is the degree of the polynomial expansion, $p(p+1)$ equations can be written.

A further reduction of the total unknowns is obtained imposing the continuity of the (micro)-stress vector on internal interfaces ($\sigma_{ij}^{(k,i_L)} n_j^{\text{int}} + \sigma_{ij}^{(r,i_L)} n_j^{\text{int}} = 0 \quad i = 1,2$) for every (k,i_L) and (r,i_L) contiguous sub-domains with a common interface of normal $\mathbf{n}^{\text{int}}$ (Figure 2-c). Therefore, additional $2(p+1)$ equations in the stress coefficients can be written for each interface, as:

$$\left(\hat{\mathbf{X}}_{ij}^{(k,i_L)}(\mathbf{y}) \hat{\mathbf{S}}^{(k,i_L)} + \hat{\mathbf{X}}_{ij}^{(r,i_L)}(\mathbf{y}) \hat{\mathbf{S}}^{(r,i_L)T} \right) n_j^{\text{int}} = 0 \quad i = 1,2 \tag{4}$$

Finally anti-periodicity of $\boldsymbol{\sigma}\mathbf{n}$ on ∂V requires $2(p+1)$ additional equations per pair of external faces (m,i_L) and (n,i_L) (Figure 2-c), so that stress vectors $\boldsymbol{\sigma}\mathbf{n}$ are opposed on opposite sides of ∂V :

$$\hat{\mathbf{X}}_{ij}^{(m,i_L)}(\mathbf{y}) \hat{\mathbf{S}}^{(m,i_L)} \mathbf{n}_{1,j} = -\hat{\mathbf{X}}_{ij}^{(n,i_L)}(\mathbf{y}) \hat{\mathbf{S}}^{(n,i_L)} \mathbf{n}_{2,j} \tag{5}$$

where $\mathbf{n}_1$ and $\mathbf{n}_2$ are oriented versors of the external faces of the paired sub-domains (m,i_L) and (n,i_L).

Elementary assemblage operations on the local variables allow to write the stress vector of layer i_L inside each sub-domain as:

$$\tilde{\boldsymbol{\sigma}}^{(k,i_L)} = \tilde{\mathbf{X}}^{(k,i_L)}(\mathbf{y}) \tilde{\mathbf{S}}^{(i_L)} \quad k = 1,\ldots, \text{ number of } sub-domains \; i_L = 1,\ldots, \text{number of } layers \tag{6}$$

where $\tilde{\mathbf{S}}^{(i_L)}$ is the vector of unknown stress parameters of layer i_L.

Equations (3), (4), (5), respectively internal equilibrium, equilibrium on interfaces and anti-periodicity, can be written in a compact form as $\mathbf{AS} = \mathbf{0}$, where $\mathbf{S}$ is the vector of the total

stress parameters. Moreover, not all the rows of this system are linearly independent and the linear dependence of some equations with respect to others can be handled easily and automatically (for instance by means of Symbolic Math Toolbox^{TM}) checking the rank of matrix **A** and progressively eliminating linearly dependent rows.

For the in-plane case, it has been shown (Milani et al. 2005) that reliable results can be obtained if a fourth order polynomial expansion is chosen for the stress field. For this reason, in all the examples treated next, expansions of degree four are adopted. Once the polynomial degree is fixed, the proposed out-of-plane model requires a subdivision (n_L) of the wall thickness into several layers (Figure 2-a), with a fixed constant thickness $\Delta_{L_i} = t / n_L$ for each layer. This allows to derive the following simple (non) linear optimization problem:

$$
\begin{cases}
\max\{\lambda\} & \\
\textit{such that} \begin{cases}
\mathbf{N} = \int_{k,i_L} \tilde{\boldsymbol{\sigma}}^{(k,i_L)} dV & (a) \\
\mathbf{M} = \int_{k,i_L} y_3 \tilde{\boldsymbol{\sigma}}^{(k,i_L)} dV & (b) \\
\mathbf{M} = \begin{bmatrix} M_{xx} & M_{xy} \\ M_{xy} & M_{yy} \end{bmatrix} = \lambda \begin{bmatrix} \cos(\psi)\cos(\vartheta) & \sin(\vartheta) \\ \sin(\vartheta) & \sin(\psi)\cos(\vartheta) \end{bmatrix} & (c) \\
\psi = [0;\, 2\pi] \quad \theta = [0;\, \pi/2] & (d) \\
\tilde{\boldsymbol{\sigma}}^{(k,i_L)} = \tilde{\mathbf{X}}^{(k,i_L)}(\mathbf{y})\tilde{\mathbf{S}} & (e) \\
\tilde{\boldsymbol{\sigma}}^{(k,i_L)} \in S^{(k,i_L)} & (f) \\
k = 1,\ldots, \text{ number of } \textit{sub-domains};\ i_L = 1,\ldots, \text{number of } \textit{layers} & (g)
\end{cases}
\end{cases}
\qquad (7)
$$

where:

- λ is the ultimate bending moment (load multiplier) with direction ψ and ϑ in the $M_{xx} - M_{yy} - M_{xy}$ space (see Figure 3);

- ψ and ϑ are spherical angles in $M_{xx} - M_{yy} - M_{xy}$, given by $\tan(\vartheta) = \dfrac{M_{xy}}{\sqrt{\left(M_{xx}^2 + M_{yy}^2\right)}}$, $\tan(\psi) = \dfrac{M_{yy}}{M_{xx}}$;

- $S^{(k,i_L)}$ denotes the (non-linear) strength domain of the constituent material (mortar or brick) corresponding to the k^{th} sub-domain and i_L^{th} layer.

- $\tilde{\mathbf{S}}$ collects all the unknown polynomial coefficients (of each sub-domain of each layer).

The following aspects of the formulation are worth noting:

- For the sake of simplicity, membrane actions are kept constant and independent from load multiplier, meaning that the effect of in-plane actions are considered only in the evaluation of M_{xx}, M_{yy}, M_{xy} strength domains. This assumption is acceptable for the tests analyzed next, since a fixed in-plane compressive load (regarded as permanent load) $N_{yy} = -N_0$ is applied before out-of-plane actions and is kept constant until failure.
- Condition (f) of equation (7) should be checked in all points of the domain V. Such check could be avoided imposing the material admissibility only where the stress status is maximum, see Belytschko and Hodge (1970). This is of course not possible for polynomial degrees larger that 1; hence, the discretisation proposed here consists in enforcing, in every sub-domain, the admissibility condition in a regular grid of "nodal points" with step rxq. Reliable solutions can be obtained with at least $3x3$ grids (see Milani et al. 2005). Obviously, in this way, a rigorous lower bound estimation of the homogenized failure surfaces is lost using interpolations with polynomial degrees larger that one, unless a second order (discontinuous) interpolation is used (see Sloan 1988). Nevertheless, it has been shown (see Milani et al. 2005) that the general procedure proposed can be adopted for obtaining accurate results.
- The non-linearity of the terms $\tilde{\boldsymbol{\sigma}}^{(k,i_L)} \in S^{(k,i_L)}$, due to the (possible) non-linearity of the strength functions of the components is avoided by means of a recursive algorithm, in order to use linear programming algorithms. On the other hand, each of the non-linear inequalities of equation (7) could be approximated by a set of linear inequalities (Anderheggen and Knopfel 1972 and Maier 1977), by replacing the yield surfaces with inscribed hyper polyhedrons. Alternatively and more efficiently, an iterative procedure is adopted here, taking advantage of the fact that the simplex method proceeds from basic solution to basic solution towards an optimal basic solution, i.e. on the vertices of the hyper polyhedron. The

basic idea of the iterative procedure (Cannarozzi et al. 1982 and Milani et al. 2005) is to adopt, in the starting step, a coarse linear approximation of the non linear failure surfaces of the components, as shown in Figure 4. The application of the simplex method in the optimization at the i^{th} step leads to an optimal solution in a corner of the domain. From the iterative i^{th} solution point a new tangent plane is added in P', as shown in Figure 4, so restarting an $(i+1)^{th}$ optimization procedure. The iterations continue until a fixed tolerance in the error between the i^{th} and $(i+1)^{th}$ solution is reached. The aim of the procedure is to give a precise approximation of the yield surface only near the solution of the problem. It is stressed here that the simplex method can rarely compete favourably with the recent and more efficient interior-point methods (IPMs) (see Krabbenhoft and Damkilde 2003). However, equation (7) has a very limited number of variables and inequality constraints, meaning that simplex-type algorithms can be profitably used to solve the problem. On the other hand, IPMs are applied next to solve the linear programming problems at a structural level, as given later by equations (9) and (12).

- In what follows, wall thickness is subdivided into at least thirty layers. Authors experienced that more refined discretizations do not allow technically meaningful improvements in the accuracy of the homogenized failure surface.

3. Finite element limit analysis of plates

The finite elements utilized for the lower and upper bound limit analyses are briefly recalled next.

- *Lower bound approach*

A FE lower bound limit analysis program based on the triangular plate bending element proposed by Hellan and Herrmann (1967) is adopted. This triangular element has been preferred rather than more accurate elements, proposed by Krenk et al. (1994) and Krabbenhoft and Damkilde (2002), due to its simplicity and the low number of unknowns involved in the

optimization. A constant moment field is assumed inside each element E, so that three moment unknowns per element are introduced; such unknowns are the horizontal, vertical and torsion moments ($M_{xx}^{E}, M_{yy}^{E}, M_{xy}^{E}$) or alternatively three bending moments M_{nn}^{Ei}, M_{nn}^{Ej}, M_{nn}^{Ek} along the edges of the triangle (Figure 5-a). Continuity of M_{nn}^{E} bending moments is imposed for each internal interface between two adjacent elements R and P (i.e. $M_{nn}^{Pj} = M_{nn}^{Rk}$, see Figure 5-b), whereas no constraints are imposed for the torsion moment and the shear force.

Due to the assumption of constant moment fields, internal equilibrium for each element is ensured only in integral form. By means of the application element by element of the principle of virtual work, three equilibrium equations for each triangle are obtained:

$$\mathbf{R}_E + \mathbf{B}_E^T \mathbf{M}_E = \mathbf{P}_E \qquad (8)$$

where

- $\mathbf{R}_E = \begin{bmatrix} R_i^E & R_j^E & R_k^E \end{bmatrix}^T$ are nodal (unknown) reactions see Figure 5-c;

- $\mathbf{B}_E = \frac{1}{2A_E} \begin{bmatrix} \frac{b_i b_i + c_i c_i}{l_i} & \frac{b_i b_j + c_i c_j}{l_i} & \frac{b_i b_k + c_i c_k}{l_i} \\ \frac{b_j b_i + c_j c_i}{l_j} & \frac{b_j b_j + c_j c_j}{l_j} & \frac{b_j b_k + c_j c_k}{l_j} \\ \frac{b_k b_i + c_k c_i}{l_k} & \frac{b_k b_j + c_k c_j}{l_k} & \frac{b_k b_k + c_k c_k}{l_k} \end{bmatrix}$, with $b_i = y_j - y_k$, $c_i = x_k - x_j$, A_E equal to the element area and l_i length of the i^{th} side;

- $\mathbf{P}_E = \frac{1}{2A_E} \mathbf{T}_E^T \int_E \begin{bmatrix} 1 & x & y \end{bmatrix}^T p(x,y) dA$ ($\mathbf{T}_E^T = \begin{bmatrix} a_i & a_j & a_k \\ b_i & b_j & b_k \\ c_i & c_j & c_k \end{bmatrix}$, $a_i = x_j y_k - x_k y_j$), which represents the lumped load equivalent to $p(x,y)$.

Further equilibrium conditions have to be imposed in order to ensure nodal equilibrium, i.e. for each (not-constrained) node i $\sum_{r=1}^{p} R_i^E = 0$, where R_i^E is referred to element E and p is the number of elements with one vertex in i. For each element E only one admissibility condition

in the linearized form $\mathbf{A}_E^{in}\mathbf{M}_E \le \mathbf{b}_{in}^E$ is required, where $\mathbf{A}_E^{in}$ is a $mx3$ coefficients matrix of the linearization planes of the strength domain, m is the number of the planes in the linearization, $\mathbf{b}_{in}^E$ collects the right hand sides of these planes and $\mathbf{M}_E = \left[M_{xx}^E \quad M_{yy}^E \quad M_{xy}^E\right]^T$ is the vector of element moment unknowns.

Finally, the following linear programming problem is obtained:

$$\max\left\{\lambda \mid \mathbf{A}^{eq}\mathbf{M} = \mathbf{b}^{eq};\ \mathbf{A}^{in}\mathbf{M} \le \mathbf{b}^{in}\right\} \qquad (9)$$

where λ is the limit multiplier, $\mathbf{M}$ is the (assembled) vector of moment unknowns (three for each element), $\mathbf{A}^{eq}\mathbf{M} = \mathbf{b}^{eq}$ collects elements equilibrium, continuity of the bending moment on interfaces, boundary conditions on bending moment and nodal equilibrium, whereas $\mathbf{A}^{in}\mathbf{M} \le \mathbf{b}^{in}$ collects linearized yield conditions (mxN^{el} inequalities if N^{el} is the number of elements).

- *Upper bound approach*

A FE upper bound limit analysis code based on the triangular element proposed by Munro and Da Fonseca (1978) is adopted. The displacement field is assumed linear inside each element and nodal velocities are taken as optimization variables. Denoting with $\mathbf{w}_E = \left[w_i^E \quad w_j^E \quad w_k^E\right]^T$ element E nodal velocities and with $\boldsymbol{\theta}_E = \left[\vartheta_i^E \quad \vartheta_j^E \quad \vartheta_k^E\right]^T$ side normal rotations, $\boldsymbol{\theta}_E$ and $\mathbf{w}_E$ are linked by the compatibility equation $\boldsymbol{\theta}_E = \mathbf{B}_E\mathbf{w}_E$ (Figure 6-a and –b). Plastic dissipation occurs only along each interface I between two adjacent triangles R and K or on a boundary side B of an element Q (see Figure 6-c).

Internal power P_I^{in} dissipated along I can be written as follows:

$$\begin{aligned} P_I^{in} &= M_{nn,I}^{+}\vartheta_I \quad \vartheta_I > 0 \\ P_I^{in} &= M_{nn,I}^{-}\left|\vartheta_I\right| \quad \vartheta_I < 0 \end{aligned} \qquad (10)$$

where

- $\vartheta_I = \vartheta_i^R + \vartheta_j^K$ is the relative rotation between R and K along I (see Figure 6-b);

- $M^{+}_{nn,I}$ and $M^{-}_{nn,I}$ are positive and negative failure bending moments along I; a rigorous upper bound of the collapse load can be obtained deducing $M^{+}_{nn,I}$ and $M^{-}_{nn,I}$ from the actual strength domain ($S^{\hom}$) of the homogenized material in the space M_{xx}, M_{yy}, M_{xy} by means of the following optimization:

$$M^{+}_{nn,I} = -M^{-}_{nn,I} = \max\left\{ \begin{matrix} M_{nn} \mid M_{nn} = M_{xx}\sin^2\Phi_I + M_{yy}\cos^2\Phi_I - M_{xy}\sin(2\Phi_I) \\ \left[M_{xx} \quad M_{yy} \quad M_{xy}\right] \in S^{\hom} \end{matrix} \right\} \qquad (11)$$

where Φ_I is the interface rotation angle with respect to the horizontal direction. A similar expression can be obtained for a boundary side B of an element Q, with the only difference that in this case $\Phi_I = \Phi^B_Q$ (see Figure 6-c).

The internal power dissipated is $P^{in} = \sum_{I}^{n^I} P^{in}_I + \sum_{B}^{n^B} P^{in}_B$, where P^{in}_B is the power dissipated on the B^{th} boundary segment. Since P^{in} is non linear, see equation (10), a non linear optimization problem is obtained. Nevertheless, this non-linearity can be easily avoided by introducing positive and negative rotations as: $P^{in}_I = M^{+}_{nn,I}\vartheta^{+}_I + M^{-}_{nn,I}\vartheta^{-}_I \quad \vartheta_I = \vartheta^{+}_I - \vartheta^{-}_I \quad \vartheta^{+}_I; \vartheta^{-}_I \geq 0$. External power dissipated can be written as $P^{ex} = \left(\mathbf{P}_0^T + \lambda\mathbf{P}_1^T\right)\mathbf{w}$, where $\mathbf{P}_0$ is the vector of (equivalent lumped) permanent loads, λ is the load multiplier, $\mathbf{P}_1^T$ is the vector of (lumped) variable loads and $\mathbf{w}$ is the vector of assembled nodal velocities. As the amplitude of the failure mechanism is arbitrary, a further normalization condition $\mathbf{P}_1^T\mathbf{w} = 1$ is usually introduced. Hence, the external power becomes linear in $\mathbf{w}$ and λ, i.e. $P^{ex} = \mathbf{P}_0^T\mathbf{w} + \lambda$.

After elementary assemblage operations, the following optimization problem is derived:

$$\min\left\{\mathbf{M}^{+T}\boldsymbol{\theta}^{+} + \mathbf{M}^{-T}\boldsymbol{\theta}^{-} - \mathbf{P}_0^T\mathbf{w} \mid \boldsymbol{\theta}^{+} - \boldsymbol{\theta}^{-} = \mathbf{B}\mathbf{w};\ \boldsymbol{\theta}^{+} \geq \mathbf{0};\ \boldsymbol{\theta}^{-} \geq \mathbf{0};\ \mathbf{P}_1^T\mathbf{w} = 1\right\} \qquad (12)$$

where;

- $\mathbf{M}^{+}$ and $\mathbf{M}^{-}$ vectors collect positive and negative failure bending moments along interfaces and boundary sides;

- $\boldsymbol{\theta}^{+}$ and $\boldsymbol{\theta}^{-}$ vectors collect positive and negative interface and boundary rotation angles;

- $\mathbf{B}$ is a geometrical matrix built up assembling $\mathbf{B}_E$ element matrices, introduced previously.

4. Out-of-plane strength for different orientations ϑ of the loading with respect to the bed joint

In this section, the ability of the homogenization procedure proposed to reproduce the strength of different masonry walls subjected to out-of-plane loads is tested for different orientations ϑ of the bending moment with respect to the bed joint direction.

A complete set of experimental strength data for specimens subjected to out-of-plane loading is given by Gazzola et al. (1985) and Gazzola and Drysdale (1986), who tested 25 wallettes of hollow concrete block masonry, with different dimensions and with the bed joints making a variable angle ϑ with the direction of loading, in four-point bending.

In order to compare experimental data with the proposed model, mechanical properties of mortar and bricks are taken in order to reproduce exactly the experimental value of f_{ft} reported by Gazzola and Drysdale (1986) for $\vartheta = 90°$. Mechanical properties of mortar and bricks are reported in Table I, whereas bricks dimensions and joints thickness are equal $390x190x150\ mm^3$ and $10\ mm$ respectively.

A comparison between experimental values and results from the numerical model for different orientation of the ϑ angle is given in Figure 7, which shows the average and standard deviation of the tests for each orientation of loading.

5. Comparison with experimental data for out-of-plane loaded panels

In this section, the proposed homogenized model is employed in order to reproduce experimental data for entire masonry panels out-of-plane loaded. In the experimental data reported next, only the tension regime is active, which means that no comparison can be made

for the out-of-plane compression regime. The experimental data available from different authors is reported in terms of maximum bending moments or flexural tensile strengths along horizontal and vertical directions. Usually, flexural tensile strengths f_t are quantities derived from experimental failure moments M_u by means of the simple elastic relation $f_t = M_u / W_{el} = 6M_u /(bh^2)$, where h is the wall thickness and b is a unitary length. Of course, such value of f_t is not the real uniaxial tensile strength, being usually defined as the flexural tensile strength. As the current model assumes fully plastic behavior, simple equilibrium equations (see Lourenço 2000) indicate that the experimental values of flexural tensile strength must be divided by 3.

5.1. McMaster University experimental tests

The first series of panels analyzed here consists of hollow concrete block masonry. The tests were carried out by Gazzola et al. (1985) and are denoted by W. Five panels were tested (WI, WII, WIII, WP1 and WF), with a height of 2800 mm and a length of 3400, 5000, 5800, 5000 and 5000 mm, respectively. The panels are all simply supported on the four edges, with the exception of panel WF (free at the top edge). The only panel with in-plane action was WP1, which differs from WII only for the compressive in-plane load. This panel was loaded, prior to the application of the out-of-plane loading, with an in-plane vertical pressure of $0.2\ N/mm^2$, which was kept constant until failure of the specimen due to the pressure p. The panels were loaded until failure with increasing out-of-plane uniform pressure p, applied by means of air-bags. For each configuration, three different tests were carried out and the results reported by the authors represent the average of the tests.

For the sake of conciseness, only the analyses conducted on panels WII, WP1 and WF are reported here. Moreover, it is stressed that, according to a previously developed incremental non-linear finite element analysis (Lourenço 2000), these panels exhibit a relatively ductile behavior and are therefore suitable for the present homogenized limit analysis.

Inelastic properties of mortar and bricks are reported in Table II, as reported by Gazzola et al. (1985). Figure 8 shows a comparison among the failure loads obtained numerically (both upper and lower bound approaches), the load-displacement diagrams obtained by Lourenço (2000) with an orthotropic elasto-plastic continuum model and experimental failure loads. It is worth noting that no information is available from Gazzola et al.(1985) regarding experimental load-displacement diagrams or scatter of the tests.

In Figure 9, the meshes utilized for the limit analyses and principal moments distributions at collapse from the lower bound analysis are shown. In Figure 10, failure mechanisms and yield line patters from the upper bound analyses are represented. The comparison shows that reliable predictions can be obtained using the homogenized model proposed.

5.2. University of Plymouth experimental tests

The second series of panels analyzed here consists of solid clay brick masonry. The tests were carried out by Chong et al (1994) and Southcombe et al (1995) and are denoted by SB. The panels analyzed next yield an additional assessment of the ability of the homogenized model to reproduce the behavior of panels with openings and made of a different masonry type. All the panels from the experiments, SB01, SB02, SB03, SB04 and SB05 are analyzed with the proposed model. Panels SB01 and SB05 are replicates and, therefore, only four different configurations are tested. Each panel, with dimensions $5600x2475x102.5\,mm^3$, was built in stretcher bond between two stiff abutments with the vertical edges simply supported (allowance for in-plane displacements was provided) and the top edge free. A completely restrained support was provided at the base because of practical difficulties in providing a simple support. The panels were loaded by air-bags until failure with increasing out-of-plane uniform pressure p. The air pressure and the displacement d for the middle point of the free edge were monitored during testing. Mechanical properties at failure adopted for the constituent materials

are given in Table III, according to Chong et al. (1994). Bricks dimensions are $215x65x102.5\ mm^3$ and joint thickness is $10\ mm$.

Figure 11 shows a comparison among collapse loads obtained with the present model, experimental pressure-displacement curves by Chong et al. (1995) and numerical pressure-displacement curves obtained by means of an orthotropic elasto-plastic macro-model (Lourenço 1997). The comparison shows that technically useful predictions on the collapse loads can be obtained simply and efficiently using the homogenized model at hand. In Figure 12, the meshes employed for the limit analyses and principal moments distributions at collapse from the lower bound analysis are reported for all the panels studied. Finally, in Figure 13 failure mechanisms and yield line patterns from the upper bound analyses are represented. Also in this case, the agreement with experimental results is worth noting.

6. Conclusions

An anisotropic homogenized model for masonry plates and shells was proposed. The model is an extension from an in plane model developed by the authors (Milani et al. 2005). The model is capable of reproducing different behavior along the material axes, which is typical of masonry behavior in flexure. The numerical calculations were compared with results available in the literature for different tests in masonry panels subjected to out-of-plane loading. Good agreement was found in all cases. The results illustrate the large possibilities of using limit analysis finite elements for the design of masonry structures subjected to out-of-plane loading. Using a relative low number of material parameters, failure loads, failure modes and distribution of internal forces can be found, using standard and efficient linear programming tools. On the other hand, some typical limitations of the limit analysis approach should be considered, as for instance its inability to predict displacements at collapse and the assumption of an infinite plastic deformation capacity of the material, hypothesis which should be checked case by case, depending both on the geometry and on the distribution of loads applied.

7. Acknowledgements

A. Tralli and G. Milani gratefully acknowledge the support of the research project MIUR COFIN 2003 – Interfacial damage failure in structural systems. Coordinator: Prof. A. Tralli.

8. References

[1] Anderheggen, E., and Knopfel, H. (1972). "Finite element limit analysis using linear programming." *International Journal of Solids and Structures*, 8, 1413-1431.

[2] Belytschko, T., and Hodge ,P.G. (1970). "Plane stress limit analysis by finite elements." *ASCE Journal of Engineering Mechanics*, December 1970, 931-943.

[3] British Standard Institution (2002). BS 5628-1:1992 Code of practice for use of masonry. Structural use of unreinforced masonry.

[4] Cannarozzi, A.A., Capurso, M., and Laudiero F. (1978). "An iterative procedure for collapse analysis of reinforced concrete plates." *Computer Methods in Applied Mechanics and Engineering*, 16, 47-68.

[5] Cannarozzi, A.A., Sacchi, P.L., and Tralli A. (1982). "On the limit analysis of steel structures in presence of shear." *Journal de Mecanique Theorique et Appliquee*, 1(3), 379-401.

[6] Chong, V.L., Southcombe, C., May, I.M. (1994). "The behaviour of laterally loaded masonry panels with openings." *Proc., 3th Int. Masonry Conf. Proc. Brit. Mas. Soc.,* London, UK, 178-182.

[7] CEN (2004), EN 1996-1-1:2002. Euro Code 6: Design of masonry structures. Common rules for reinforced and unreinforced masonry structures.

[8] Gazzola, E.A., and Drysdale, R.G. (1986). "A component failure criterion for blockwork in flexure." *Structures '86 ASCE,* edited by S.C. Anand, New Orleans, Louisiana, USA, 134-153.

[9] Gazzola, E.A., Drysdale, R.G., and Essawy , A.S. (1985). “Bending of concrete masonry walls at different angles to the bed joints.” *Proc. 3th North. Amer. Mas. Conf.*, Arlington, Texas, USA, Paper 27.

[10] Hellan, K. (1967). “Analysis of elastic plates in flexure by a simplified finite element method.” *Acta Polytech. Scand.*, Trondheim, Ci 46, 1-28.

[11] Herrmann, L.R. (1967). “Finite element bending analysis for plates.” *J. Eng. Mech. Div.* ASCE, 93, 13-26.

[12] Hodge, P.G. (1959). *Plastic analysis of structures*, McGraw Hill.

[13] Krabbenhoft, K., and Damkilde., L. (2002). “Lower Bound limit analysis of slabs with nonlinear yield criteria.” *Computers and Structures*, 80, 2043-2057.

[14] Krabbenhoft, K., and Damkilde, L. (2003). “A general nonlinear optimization algorithm for lower bound limit analysis.” *Int. Jour. for Num. Meth. in Eng*., 56, 165-184.

[15] Krenk, S., Damkilde, L., and Hoyer, O. (1994). “Limit analysis and optimal design of plates with equilibrium elements.” *J. Eng. Mech. ASCE*, 120(6), 1237-1254.

[16] Lourenço, P.B. (1997). “An anisotropic macro-model for masonry plates and shells: implementation and validation.” *Report 03.21.1.3.07*, University of Delft, Delft, Holland and University of Minho, Guimarães, Portugal. Available from www.civil.uminho.pt/masonry.

[17] Lourenço, P.B. (2000). “Anisotropic softening model for masonry plates and shells.” *Jour. Struct. Eng. ASCE*, 126(9), 1008-1016.

[18] Maier, G. (1977). “Mathematical programming methods for deformation analysis at plastic collapse.” *Computers and Structures*, 7, 599-612.

[19] Milani, G., Lourenço, P.B., and Tralli A. (2005). “Homogenised limit analysis of masonry walls. Part I: failure surfaces.” *Computers & Structures, accepted for publication*.

[20] Munro, J., and Da Fonseca, A.M.A. (1978). “Yield-line method by finite elements and linear programming.” *J. Struct. Eng. ASCE*, 56B, 37-44.

[21] Sinha, B.P. (1978). “A simplified ultimate load analysis of laterally loaded model orthotropic brickwork panels of low tensile strength.” *J. Struct. Eng. ASCE*, 56B(4), 81-84.

[22] Sloan, S.W., (1988). “Lower bound limit analysis using finite elements and linear programming.” *Int. Jour. Num. and Anal. Meth. Geomech*., 12, 61-67.

[23] Southcombe, C., May, I.M., and Chong, V.L. (1995). “The behaviour of brickwork panels with openings under lateral load.” *Proc., 4th Int. Masonry Conf. Proc. Brit. Mas. Soc.*, London, UK, 1, 105-110.

[24] Spence, R., and Coburn, A. (1992). “Strengthening building of stone masonry to resist earthquakes.” *Meccanica*, 27, 213-221.

[25] Suquet, P. (1983). “Analyse limite et et homogeneisation.” *Comptes Rendus de l'Academie des Sciences - Series IIB – Mechanics*, 296, 1355-1358.

Notation

$\mathbf{A}_E^{in}$ $mx3$ coefficients matrix of the linearization planes of the strength domain, element E

$\mathbf{b}_{in}^E$ right hand sides of the linearization planes, element E

$\mathbf{B}_E$ geometric matrix of element E

c_m mortar cohesion

E triangular element

f_{cb} brick compressive cut-off

f_t flexural masonry strength

f_{tm} mortar tension cut-off

h wall thickness

I interface between adjacent triangles

(i_L) i^{th} layer

(k) sub domain

$\mathbf{M}$ macroscopic out-of-plane tensor

$\mathbf{M}^+$ ($\mathbf{M}^-$) assembled vector of positive (negative) failure bending moments

M_u (M_{uh}) ultimate experimental (horizontal) bending moment

$M_{xx}^E, M_{yy}^E, M_{xy}^E$ moments

M_{nn}^{Ei}, M_{nn}^{Ej}, M_{nn}^{Ek} edge bending moments

$\mathbf{n}$ outward versor of ∂Y_l

$\mathbf{n}^{\text{int}}$ normal to an internal interface

$\mathbf{N}$ macroscopic in-plane tensor

$p(x, y)$ out-of-plane load

P^{ex} total external power

P^{in} internal power

P_I^{in} internal power dissipated along I

$\mathbf{P}_E$ lumped external out-of-plane load for element E

$\mathbf{R}_E$ vector of nodal reactions of element E

S^{m} (S^{b}) mortar (brick) strength domain

$S^{(k,i_L)}$ (non-linear) strength domain, k^{th} sub-domain, i_L^{th} layer.

S^{hom} homogenized strength domain

$\tilde{\mathbf{S}}$ unknown polynomial coefficients

V elementary cell

$\mathbf{w}_E$ nodal velocities, element E

Y cross section of elementary cell with $y_3 = 0$

$|Y|$ Y area

∂Y_l internal boundary surface of the elementary cell

Δ_{i_L} i^{th} layer thickness

ϑ angle

$\boldsymbol{\theta}_E$ side normal rotations, element E

λ load multiplier

Φ_I interface rotation angle with respect to the horizontal direction

Φ_m mortar friction angle

$\boldsymbol{\sigma}$ microscopic stress tensor

$[\![\boldsymbol{\sigma}]\!]$ jump of micro-stresses across $\mathbf{n}^{\text{int}}$

Ω generic masonry panel

ψ angle

Figures

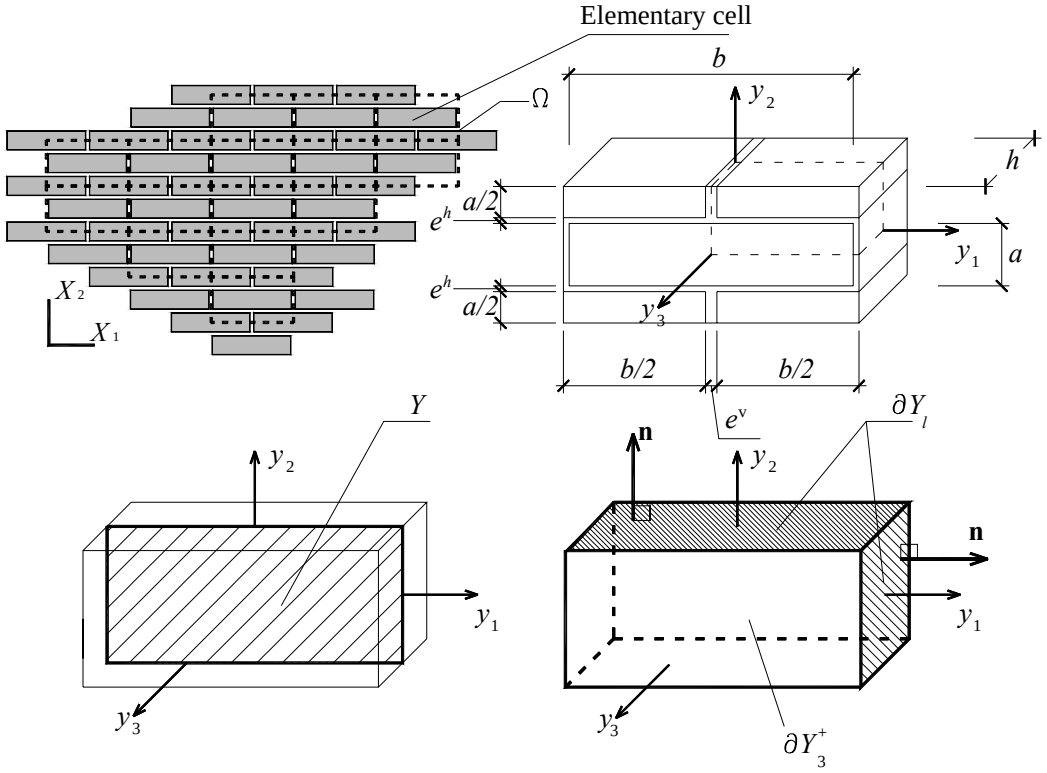

Figure 1: Periodic structure ($X_1 - X_2$: macroscopic frame of reference) and elementary cell ($y_1 - y_2 - y_3$: local frame of reference).

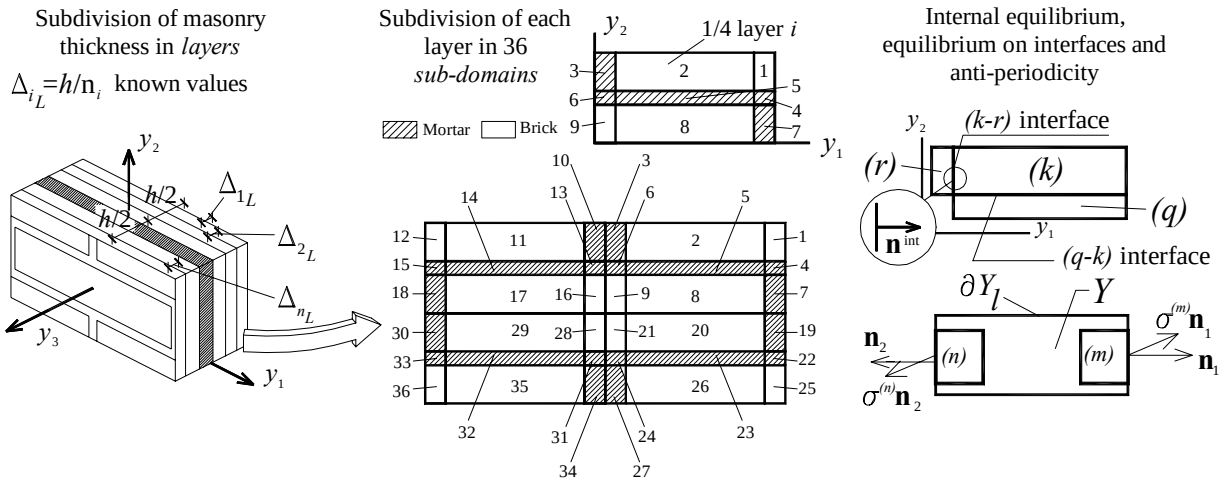

-a -b -c

Figure 2: The micro-mechanical model proposed. -a: subdivision in layers along the thickness. –b: subdivision of each layer in sub-domains. –c: imposition of internal equilibrium, equilibrium on interfaces and anti-periodicity.

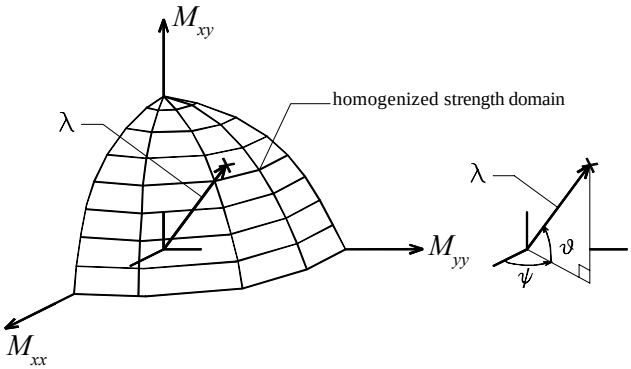

Figure 3: Meaning of λ multiplier in the optimization problem and ψ and ϑ angles.

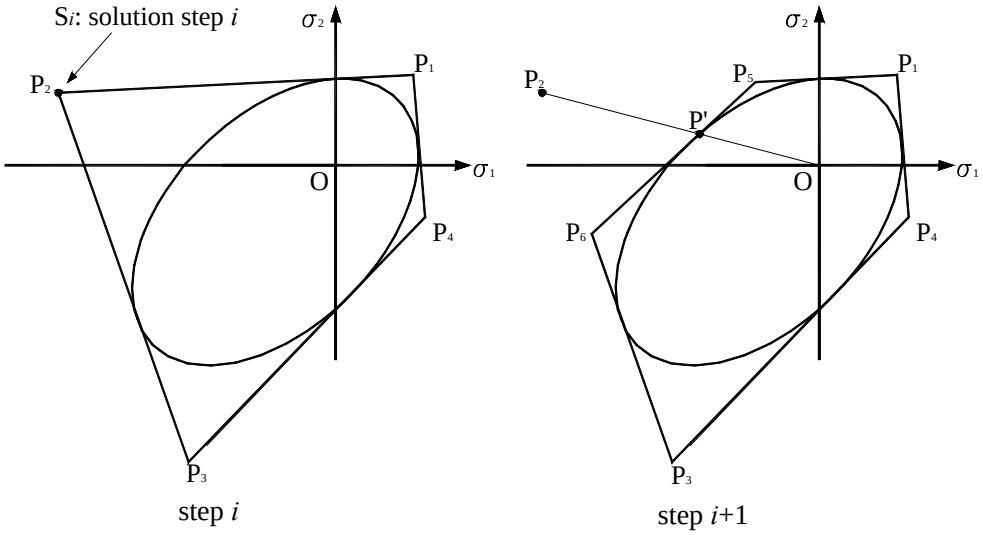

-a -b

Figure 4: Iterative procedure utilized in the optimization problem. –a: step *i*; -b: step *i*+1.

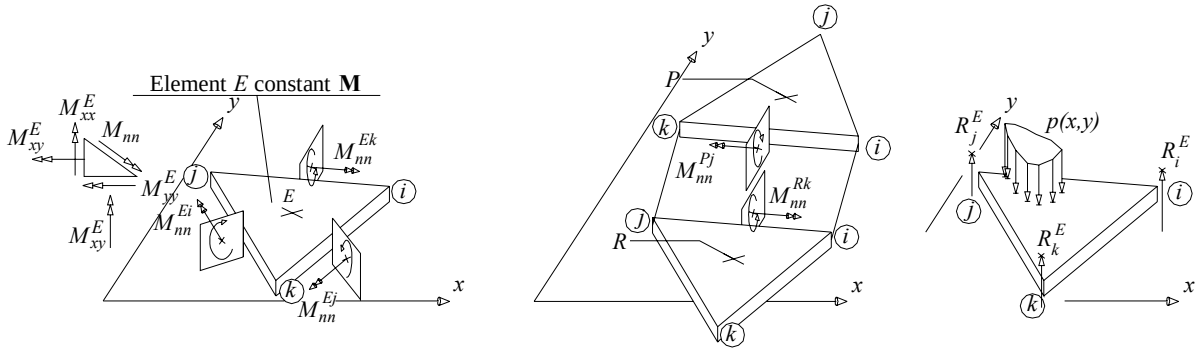

-a -b -c

Figure 5: Triangular plate element used for the lower bound FE limit analysis (-a), continuity of the bending moment on interfaces (-b), integral equilibrium (-c).

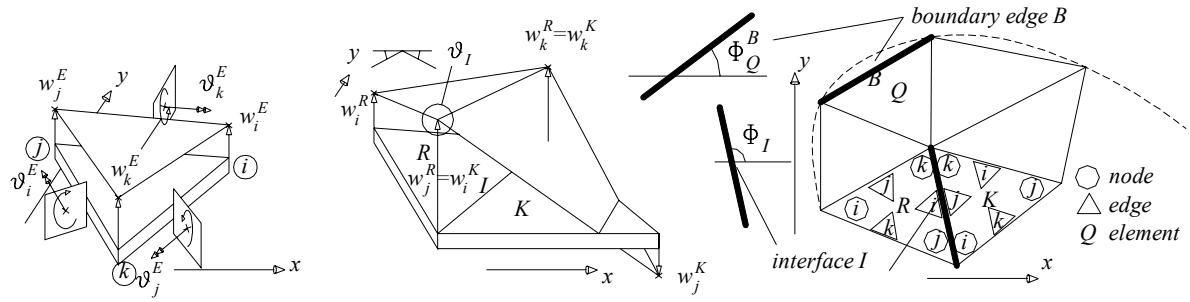

-a -b -c

Figure 6: Triangular plate element used for the upper bound FE limit analysis (-a), rotation along an interface between adjacent triangles (-b), discretization of the 2D domain (-c).

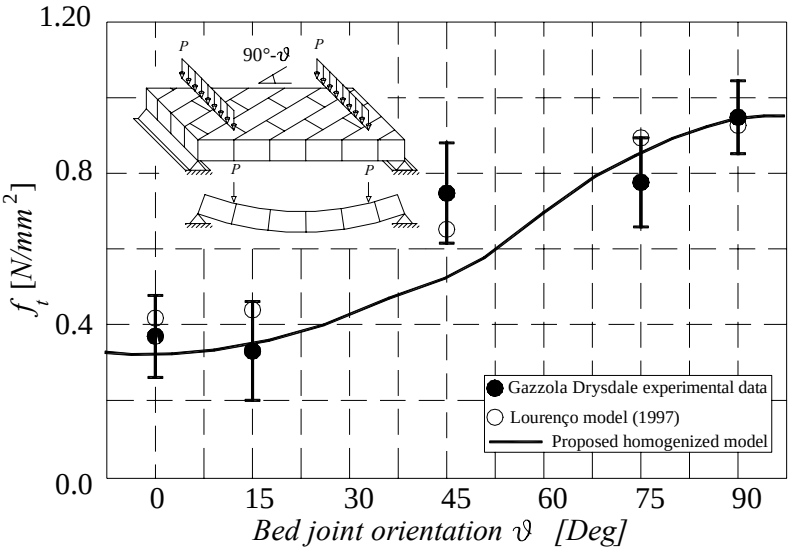

Figure 7: Comparison among experimental results by Gazzola and Drysdale (1986), plasticity model by Lourenço (2000) and proposed model for the evaluation of flexural strength at different values of ϑ angle.

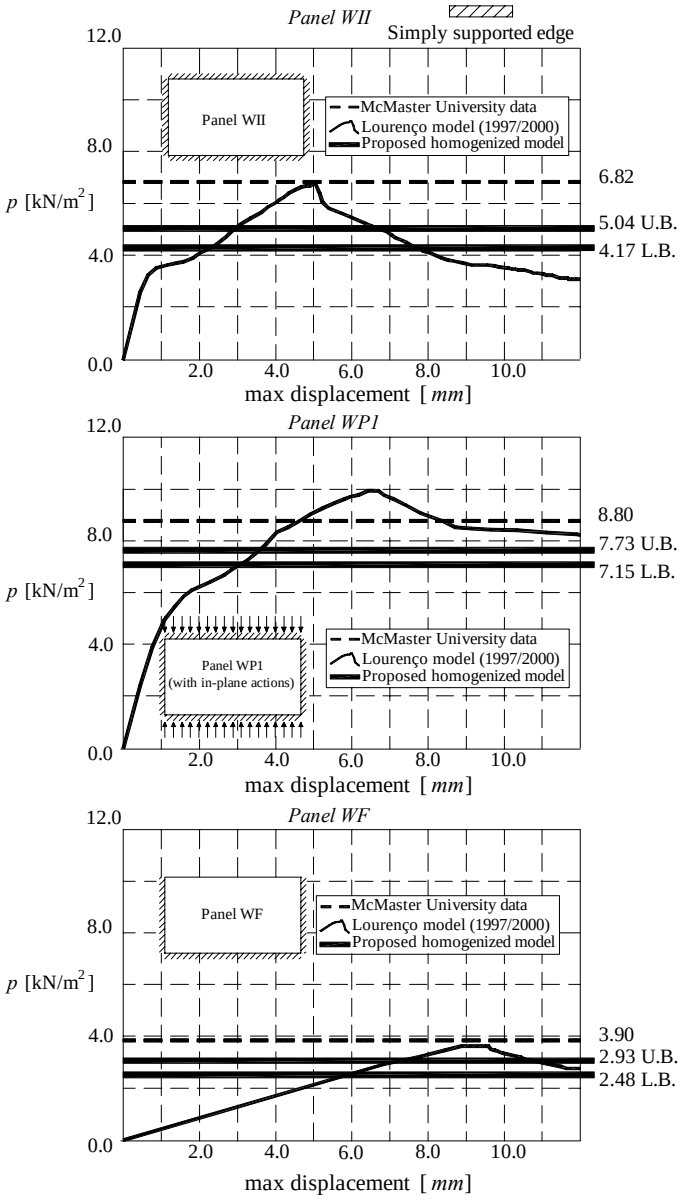

Figure 8: Comparison between experimental and numerical results obtained, University of McMaster experimental tests, panels WII WPI WF.

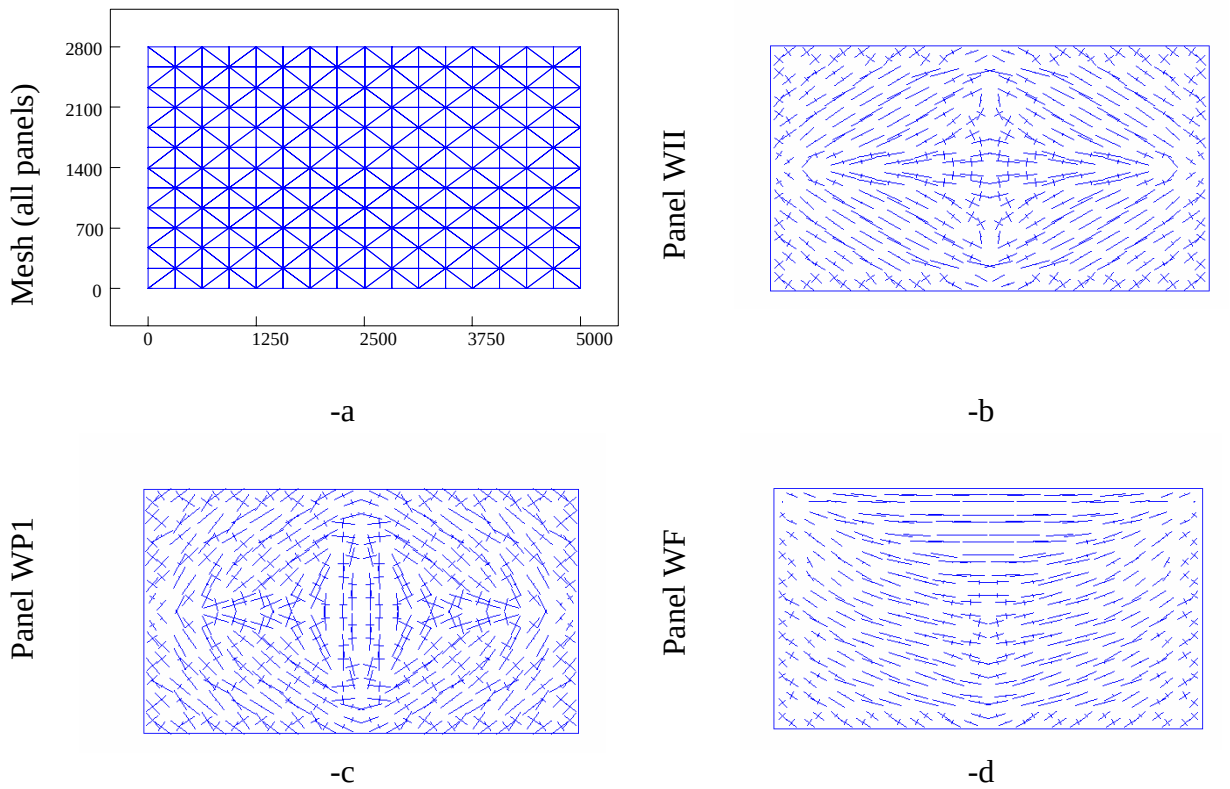

Figure 9: University of McMaster experimental tests, lower bound FE limit analysis. –a: mesh used for panels WII WPI WF. Principal moments at collapse, -b: panel WII, -c: panel WP1; -d: panel WF.

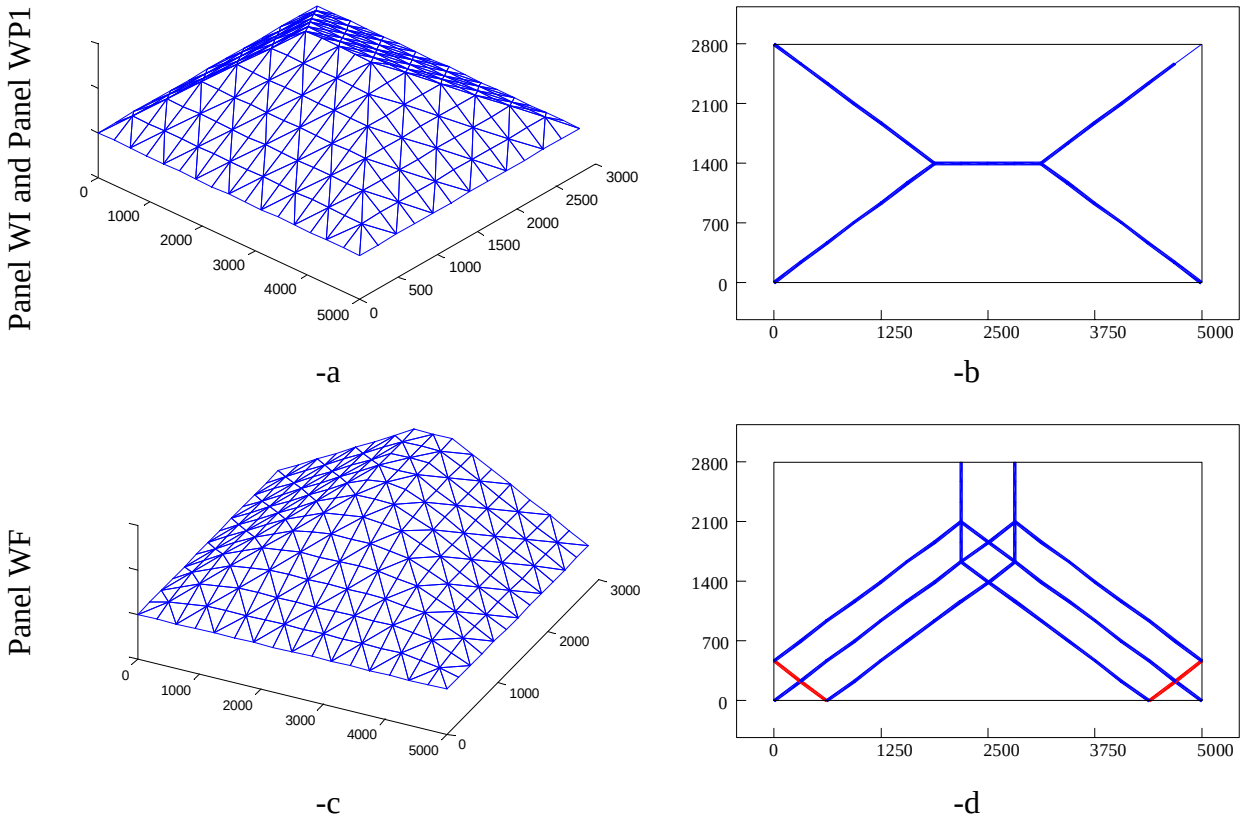

Figure 10: University of McMaster experimental tests, upper bound FE limit analysis. –a: panels WII and WP1 deformed shape at collapse. –b: panels WII and WP1 yield lines pattern. –c: panel WF deformed shape at collapse. –d: panels WF yield lines pattern.

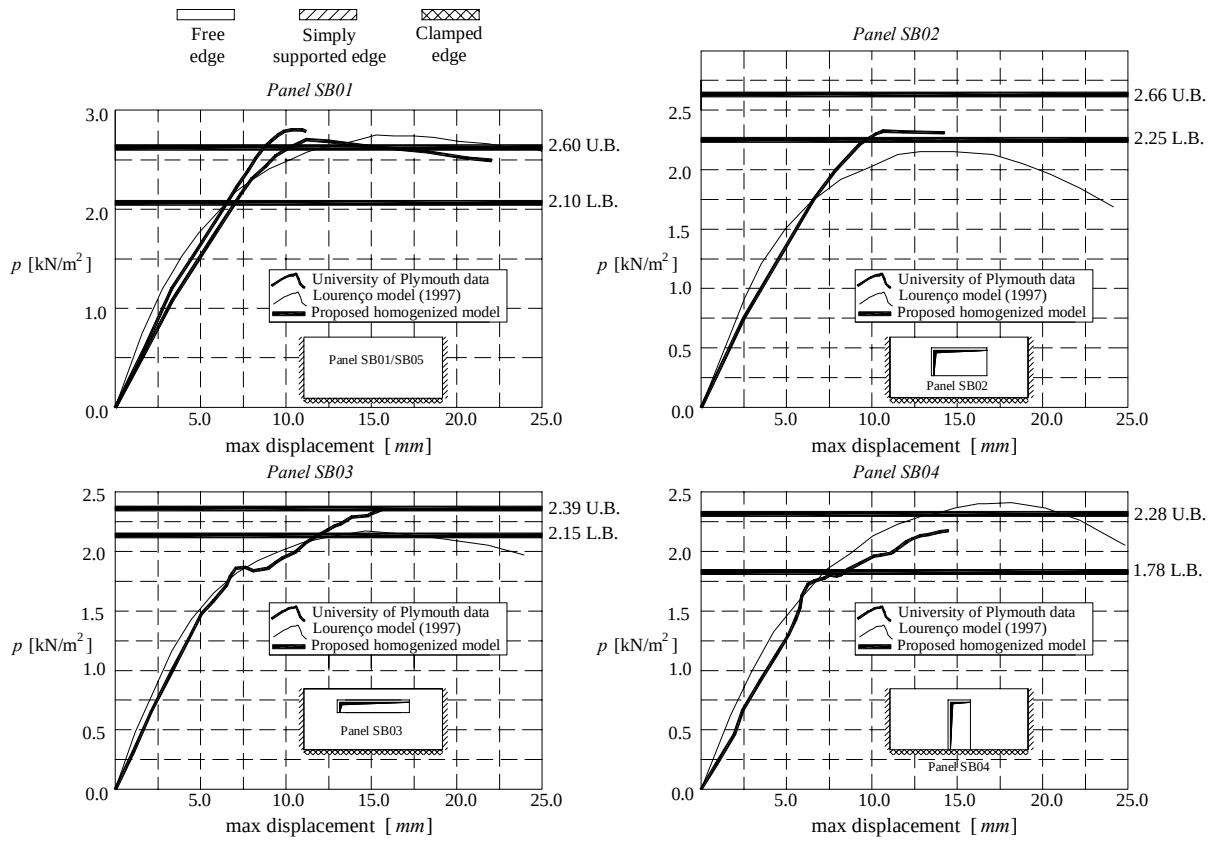

Figure 11: Comparison between experimental and numerical results obtained, University of Plymouth experimental tests.

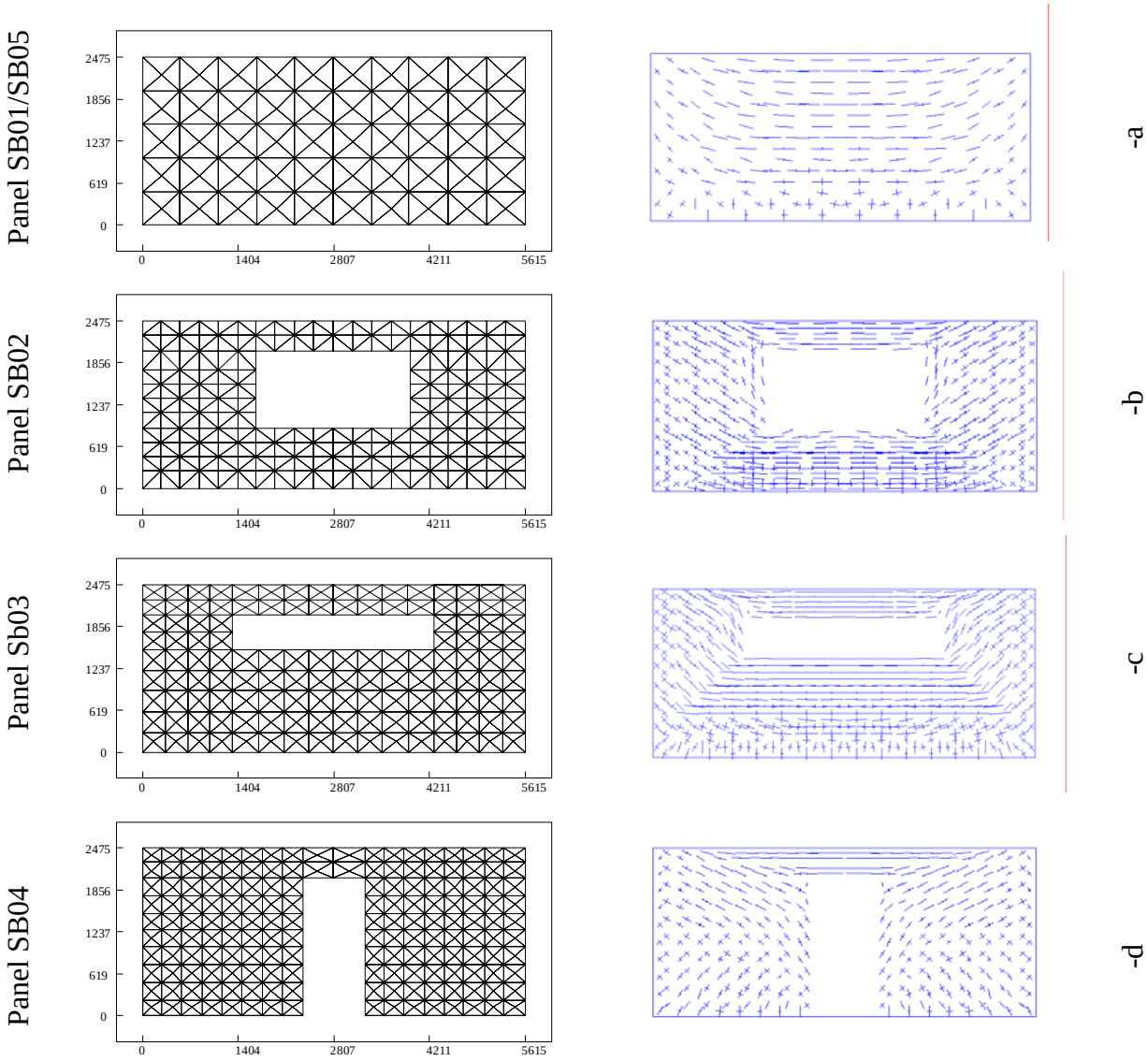

Figure 12: University of Plymouth experimental tests, meshes used for the analyses and lower bound FE limit analysis results (principal moments at collapse). –a: Panel SB01/SB05; -b: Panel SB02; -c: Panel SB03; -d: Panel SB04.

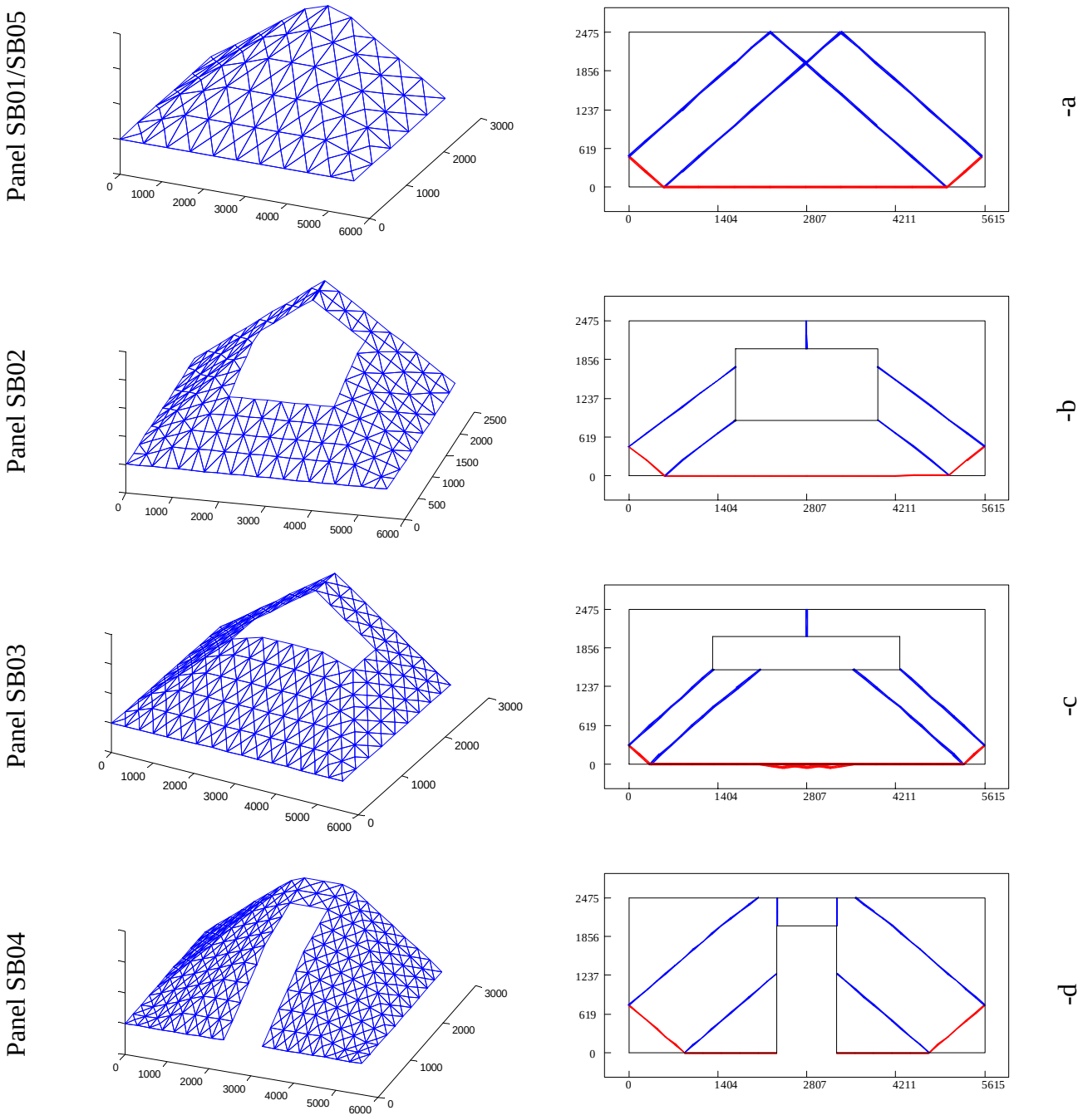

Figure 13: University of Plymouth experimental tests, upper bound FE limit analysis results (deformed shape at collapse and yield lines patterns). –a: Panel SB01/SB05; -b: Panel SB02; -c: Panel SB03; -d: Panel SB04.

Tables

Table I: Comparison with experimental data by Gazzola and Drysdale (1986) on concrete block wallettes. f_{tm} : mortar tension cut-off; c_m : mortar cohesion, Φ_m : mortar friction angle, f_{cb} : brick compressive cut-off.

Data assumed for the homogenized model	
Mortar (thickness: 10 mm)	*Brick (height x width 190mm x 390mm) Wallettes thickness 150 mm*
Mohr Coulomb plane strain with tension cut-off $f_{tm} = M_{uh} / (h^2 / 6) \quad \left[\frac{N}{mm^2} \right]$ (tension cut-off) $c_m = 2 f_{tm}$ (cohesion) $\Phi_m = 36°$ (friction angle)	Compression cut-off $f_{cb} = 22.7 \frac{N}{mm^2}$

Table II: Comparison with experimental data by Gazzola et al. (1985) on out-of-plane loaded panels. f_{tm} : mortar tension cut-off; c_m : mortar cohesion, Φ_m : mortar friction angle, f_{cb} : brick compressive cut-off.

Mechanical and geometrical characteristics assumed	
Mortar (thickness: 10 mm)	*Brick (height x width 190mm x 390mm) Wall thickness 150 mm*
$f_{tm} = 0.157 \frac{N}{mm^2}$ (tension cut-off) $c_m = 3.8 f_{tm}$ (cohesion) $\Phi_m = 36°$ (friction angle)	$f_{cb} = 22.7 \frac{N}{mm^2}$

Table III: Comparison with experimental data by Chong et al. (1995) on out-of-plane loaded panels. f_{tm} : mortar tension cut-off; c_m : mortar cohesion, Φ_m : mortar friction angle, f_{cb} : brick compressive cut-off.

Mechanical characteristics assumed	
Mortar	*Brick*
Mohr Coulomb plane strain with tension cut-off (thickness 10 *mm*) $f_{tm} = 0.32 \frac{N}{mm^2}$ (tension cut-off) $c_m = 1 f_{tm}$ (cohesion) $\Phi_m = 36°$ (friction angle)	Compression cut-off $f_{cb} = 20 \frac{N}{mm^2}$